Increasing the Predictability of AIMS™ Measurements by Coupling to Resist Simulations

Balint Meliorisz[1,2], Andreas Erdmann[2], Thomas Schnattinger[2], Ulrich Strößner[3], Thomas Scherübl[3], Peter De Bisschop[4], and Vicky Philipsen[4]
[1]Chair of Electron Devices, Friedrich-Alexander University Erlangen-Nuremberg, Cauerstr. 6, 91058 Erlangen, Germany
[2] Fraunhofer-Institute of Integrated Systems and Device Technology (IISB), Schottkystrasse 10, 91058 Erlangen, Germany
[3] Carl Zeiss SMS GmbH, Carl Zeiss Promenade 10, 07745 Jena, Germany
[4] IMEC, Kapeldreef 75, 3001 Leuven, Belgium

ABSTRACT

This paper studies the application of resist models to AIMS™ [1] images. Measured AIMS™ data were coupled with resist simulations of the Fraunhofer IISB research and development lithography simulator Dr.LiTHO [2] and with a compact resist model developed by Carl Zeiss SMS. Through-focus image data of the AIMS™ are transformed into a bulk image - the intensity distribution within the resist. This bulk image is used to compute the concentration of photo-acid after exposure and the following resist processing. In the result a resist profile is obtained, which can be used to extract the printed wafer linewidth and other data. Additionally, a compact resist model developed by Carl Zeiss SMS was directly applied to the AIMS™ data. The described procedures are used to determine dose latitudes for lines and spaces with different pitches. The obtained data are compared to actual wafer prints for a 1.2 NA system.

Keywords: AIMS, Hyper-NA imaging, lithography simulation, resist modeling, mask inspection

1. INTRODUCTION

Rigorous electromagnetic field simulation of light diffraction from the mask in combination with image and resist simulation is used to predict the lithographic performance for given mask geometries and optical material parameters [3]. This enables comprehensive simulation studies for the evaluation and optimization of mask absorber stacks and the estimated lithographic performance of a photomask. Lithography simulation relies on an accurate input of the mask geometry and material parameters. In contrast to that, the AIMS™ measures the projected image of a fabricated mask taking into account real-world parameters such as optical constants in potentially inhomogeneous absorber stacks, side wall angles, corner rounding, or line edge roughness of an absorber feature.

For more than 10 years AIMS™ has been a well established methodology in the mask shop as a quasi industry standard. The mask is illuminated under the same wavelength and illumination conditions (NA, sigma and off-axis pattern) as in a scanner (see Figure 1). The light diffracted by the mask is gathered by an objective lens which also has the same NA on mask level as a corresponding scanner. This lens magnifies the image of the mask onto a CCD camera. Thus, the camera captures the aerial image of the mask under the same conditions as a scanner will see it or in other words the scanner is emulated by using an AIMS™. Defects and mask features like OPC can precisely be evaluated by an AIMS™ tool concerning printability on the wafer. Therefore, this method is well established in the mask shop mainly for defect disposition and repair verification under scanner conditions without the need of wafer prints.

The latest generation of the AIMS™ tool family is the AIMS™ 45 – 193i [4] which has been designed to emulate immersion scanners with an NA up to 1.4. The insertion of immersion lithography for the 45nm node required a completely new set of specifications for AIMS™. Higher NA and sophisticated polarized (azimuthal) illumination schemes as used in immersion scanners have been implemented into the new tool platform.

Additionally, the tool is equipped with the new Zeiss proprietary vector effect emulator which allows to emulate the

contrast of aerial images in resist which are formed under high angles. The contrast loss in the resist cannot be described by an AIMS™ alone as the AIMS™ has a magnifying lens which results in a low NA at the camera side. Therefore, for the AIMS™ 45 – 193i the scanner mode has been developed which generates from several AIMS™ images an image-in-resist and takes into account the contrast loss due to vector effects. The scanner mode has been extensively tested by comparing AIMS™ results in scanner mode to wafer prints. Excellent agreement has been reported in recent publications [5,6,7]. However, the capture of the aerial image does naturally not take into account effects which are due to the resist process like diffusion length, Dill parameters, or others.

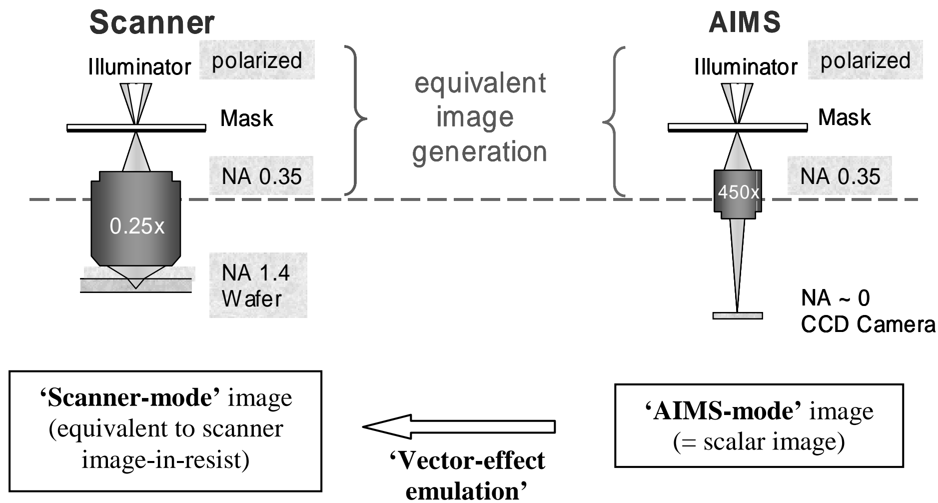

Figure 1: *Comparison of the operation of an AIMS™ system with a wafer scanner. At reticle-side, both systems are equivalent, but the AIMS™ uses a magnifying lens, whereas the scanner demagnifies. The result is that as-measured AIMS™ images are basically 'scalar' images. The 'vector-effect emulator' used in the so-called 'scanner mode' of the new AIMS™45-193i, however, converts the measured images into a scanner-equivalent image, i.e. into a prediction of the intensity distribution inside the resist in the scanner.*

In order to close the gap from the aerial image-in-resist which is implemented in the AIMS™ 45 – 193i tool as scanner mode to the wafer prints, in this work the application of resist models to the measured AIMS™ images has been studied.

The paper is organized as follows: Section 2 reviews different resist modeling approaches and introduces a new compact resist model which is directly applied to measured AIMS™ data. Afterwards, the coupling of measured AIMS™ data with standard resist models is described. Section 4 compares wafer prints with modeling results which are obtained with different resist models. The paper concludes with a summary and outlook on future work.

2. PHOTORESIST MODELING APPROACHES

The different degrees to which the physics and chemistry of various lithographic processing steps is understood has motivated the development of resist simulation models at different levels of abstraction. Mesoscopic models describe the photoresist processing by tracking discrete relevant photoresist molecule concentrations during photoresist processing steps [8]. Such models can be used to predict the impact of the discrete composition of the photoresist, the finite size of molecules, and the inherently stochastic nature of particle behavior on stochastic process fluctuations, causing the so-called line edge roughness (LER) and other phenomena. This main application of the mesoscopic resist models is beyond the purpose of this paper. This section reviews the resist models which were used for the purpose of this study.

2.1 FULL RESIST MODELS

Similar to mesoscopic models, macroscopic or continuous photoresist models are based on a sequential simulation of single lithographic process steps. In these models, relevant photoresist components such as photoacid generators PAG, photoacids A, quencher bases B, and inhibitor groups M are specified by continuous concentration values. In the following the concentration of a chemical component X inside the resist is represented by the symbol [X].

The chemical modification of the photoresist during the exposure is described by the well established Dill-model:

$$\frac{\partial[PAG]}{\partial t} = -C_{eff} \cdot I \cdot [PAG] \qquad (1.1)$$

$$\alpha = A_{Dill} \cdot [PAG] + B_{Dill} \qquad (1.2)$$

Here the letter "I" represents the intensity distribution of the light inside the resist, which depends on the light which is projected onto the wafer and on the optical properties (refractive index n and absorption coefficient α) of the resist and the materials in the wafer stack. C_{eff} is the acid generation efficiency of the resist material. The absorption coefficient α of the resist depends on the bleachable absorption A_{Dill} and the unbleachable absorption B_{Dill}. The upper equations are solved with the initial condition $[PAG]_{t=0}=1.0$. The concentration of photoacid [A] after the exposure is obtained from

$$[A] = 1 - [PAG] \qquad (2)$$

During the post-exposure-bake (PEB) the photogenerated acid deprotects inhibitor groups. In addition to that, also thermal induced deprotection reactions may occur. The acid acts as a catalyzer and is not consumed in the deprotection reaction. However, acid can be neutralized by quencher bases or spontaneous acid loss can occur. Moreover, the acid and the quencher base diffuse inside the resist. In general, the diffusivity or mobility of the acid and the quencher depend on the concentration of protected inhibitor groups.

Following these assumptions, the coupled diffusion kinetic reactions can be described by the following system of partial differential equations [9]:

$$\frac{\partial[M]}{\partial t} = -k_1 \cdot [M]^p \cdot [A]^q - k_2 \cdot [M] \qquad (3.1)$$

$$\frac{\partial[A]}{\partial t} = -k_3 \cdot [A]^r - \nabla\left(D_A([M])\nabla[A]\right) - k_4 \cdot [A] \cdot [B] \qquad (3.2)$$

$$\frac{\partial[B]}{\partial t} = -\nabla\left(D_B([M])\nabla[B]\right) - k_4 \cdot [A] \cdot [B] \qquad (3.3)$$

The initial condition for the numerical solution of this equation is given by the photoacid concentration [A] after the exposure and by the (initial) concentrations of quencher base [B] and inhibitor [M], respectively. The model parameter k_1 is the rate constant for acid catalyzed deprotection and k_2 the rate constant accounting for thermally induced deprotection. The latter term determines the dark erosion rate of the inhibitor in the resist after PEB. Exponents p, q are reaction orders of each species. Equation (3.2) describes irreversible acid loss effects, acid diffusion, and acid-quencher neutralization. r is an effective reaction order and k_3 is the photoacid loss reaction rate; k_4 indicates the photoacid neutralization rate. The diffusion coefficients of acid D_A and quencher D_B depend on free volume, concentration of protected sites [M], and on other parameters. If D_X is independent from the concentration of the inhibitor we speak of Fickian diffusion.

The solubility of the photoresist material is characterized by a rate function R([M]). Different forms of rate functions such as Mack, enhanced Mack and Weiss-model were proposed in literature [10]. For the scope of this article we restricted ourselves to the most often used Mack-model [11].

$$R([M]) = R_{max} \cdot \left[\frac{(a+1)\cdot(1-[M])^n}{a+(1-[M])^n} \right] + R_{min} \tag{4}$$

$$\text{with} \qquad a = \frac{n+1}{n-1}\cdot(1-M_{th})^n$$

R_{min} and R_{max} specify the minimum and maximum development rate of the photoresist, n characterizes the steepness of the rate curve, M_{th} specifies the value of [M] where the dissolution "turns on".

Equations (1) to (4) specify a full resist model (FRM). Although this model covers the impact of many important photoresist processing effects, it is often difficult to apply to real processes. Most of the model parameters strongly depend on the specific type of resist and on processing conditions and are difficult to measure. Therefore, extensive parameter calibration is required to adapt a FRM to a real process.

2.2. EFFECTIVE ACID RESIST MODELS

In order to reduce the complexity of the full resist model an effective acid resist model was proposed [12]. It neglects details of the coupled deprotection diffusion reactions according to equation (3). The development rate is obtained as a function of the (effective) acid concentration. Diffusion and quencher base effects are taken into account by a fast (partial) neutralization of the photogenerated acid and the convolution of the remaining acid distribution with a Gaussian kernel function which is characterized by the diffusion length dl.

$$[A_{eff}] = \max([A]-[B],0) \otimes K(dl) \tag{5}$$

where [B] stands for the the initial quencher base concentration. The development rate equation is applied to an effective acid concentration $[A_{eff}]$ instead of [M].

The described effective acid resist model (EARM) can be used to simulate 2D/3D resist profile topographies. Although it neglects details of the deprotection reaction, it covers the most important resist effects. Compared to the FRM it has a considerably lower number of parameters.

2.3 COMPACT RESIST MODELS

For certain applications it is sufficient to describe the photoresist as a simple threshold detector. The threshold resist model is applied to the simulated or measured aerial images. These are intensity distributions in one focal plane inside air, immersion liquid, or photoresist, which are normalized with respect to an open frame exposure. After the resist processing, a positive-tone photoresist is removed at all positions where the aerial image intensity is larger than the threshold (typically between 0.1 and 0.3 relative to the total illumination intensity). The feature sizes and positions are obtained from the corresponding contours of the aerial image at the specified threshold. The threshold resist model can be used for a fast qualitative evaluation of the impact of mask and optical system parameters on the lithographic process. This kind of threshold analysis is currently used in the AIMS™ software e.g. for evaluation of defects regarding their impact on CD variation. A threshold resist model does not cover the impact of photoresist kinetic, diffusion, and development effects. This may cause some deviation in the quantitative description of lithographic parameters like e.g. iso-dense-bias or sidelobe printability.

Different types of compact models were developed to cover the impact of the photoresist on the resulting feature sizes in a more accurate way. In these models, photoresist phenomena such as diffusion or quencher effects are emulated by the application of simple mathematical operations on the aerial image. Fuard et al. [13] applied a simple Gaussian diffu-

sion to aerial image data. A more general model – the so called acid dose diffusion threshold model (ADDIT) [14] and extensions thereof [15] were developed to cover additional resist effects such as chemical amplification, acid-quencher neutralization, and quencher diffusion. Compact resist models rely on a small number of model parameters (<= 4) which are obtained by a fit of experimental data for given process settings. In most cases these compact resist models provide a good quantitative description of lithographic processes for given process settings, such as NA, illumination, wafer stack, pre-exposure-bake, and post-exposure bake.

The application of multi-parameter resist models to AIMS™ measurements has some practical limitations as the AIMS™ is mainly used in the mask shop for defect disposition. Mask shops usually do not have access to resist parameters or calibration models of their customers, the wafer fabs. On the other hand for smaller future nodes it might become necessary to take resist effects into account for improved defect analysis. For that purpose a special compact resist model AIMS-CRM with a focus on typical AIMS applications has been developed by Carl Zeiss SMS. In contrast to FRM and EARM which evaluate the aerial image at several effective focus positions inside the photoresist AIMS-CRM considers the aerial image at one focus position inside the resist only. Photoacid generation, diffusion, and quencher base effects are described by an approach similar to that one used in the ADDIT-model [14]. The dissolution rate equation (4) is replaced by a step function using an inhibitor concentration threshold. In this study the resist model AIMS-CRM is compared to other resist models and to wafer prints.

3. COUPLING OF AIMS AND RESIST SIMULATIONS

This section describes the coupling of AIMS™ data and the resist models of Dr.LiTHO. Full resist profile simulations using FRM and EARM rely on the input of the intensity distribution inside the resist – the so called bulk image. Accurate resist simulation requires the input of the bulk image at an equidistant grid with a spatial resolution below 2nm. AIMS™ enables the measurement at several discrete focus positions. An extension of the scaled defocus approach of Bernard [16] was used to transfer the AIMS™ data at discrete focus positions into a continuous intensity distribution inside the resist. Figure 2 demonstrates the resulting procedure.

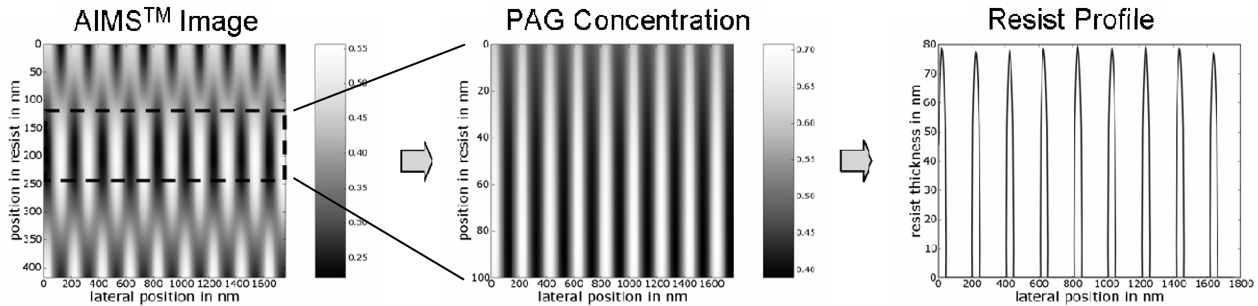

Figure 2: *Coupling of measured AIMS™ images to full resist simulations: Interpolation of AIMS™ data at different focus position is used to compute scaled defocus intensity data. The relevant range of intensity values (dashed box) is determined by the focus position of the scanner and by the thickness of the photoresist. These intensity data are used to compute the concentration of photoacid generator (center) inside the resist after exposure. Application of standard full resist models results in a resist profile (right).*

First, the focus position f_{AIMS} of the AIMS™ data are converted into focus positions inside the photoresist f_{res}:

$$f_{res} = f_{AIMS} \frac{n_{iml} - \sqrt{n_{iml}^2 - NA^2}}{n_{res} - \sqrt{n_{res}^2 - NA^2}} \approx f_{AIMS}\, n_{res} / n_{iml} \qquad (6)$$

n_{iml} and n_{res} are the refractive indices of the immersion liquid and the resist respectively. In contrast to the original scalar method of Bernard the polarization dependent imaging effects are taken into account by the Zeiss proprietary vector effect emulator, the so-called AIMS™ scanner mode. To perform full resist model simulations at several focus positions, the AIMS™ data have to be measured over a sufficiently large range of focus positions. Next, the AIMS™ data have to be converted to the grid which is required for the resist simulation. This is done by standard interpolation techniques. The image intensity inside the photoresist is given by a range of effective focus positions inside the resist f_{res} - see dashed box in the left part of Figure 2. The size and position of this range are defined by the resist thickness and by the focus position f_{scan} of the lithographic projection scanner.

The absorption of modern chemically amplified resists does (almost) not change during the exposure. The parameter A_{Dill} in equation (1.2) is very close to zero. This results in a time independent intensity distribution inside the photoresist and the solution of equation (1.1) is given by

$$[PAG] = [PAG_0] \cdot \exp\left(-C_{eff} I \cdot t_{exp}\right) \tag{7}$$

$[PAG_0]$ is the concentration of photoacid generators before the exposure step, which is usually normalized to 1. t_{exp} symbolizes the exposure time. The product $I \cdot t_{exp}$ can by summarized as the local dose. The center part of Figure 2 shows the computed PAG distribution inside the photoresist for bulk image intensity in the solid box in the left part of Figure 2. This PAG distribution is used as starting value for the simulation of the post-exposure-bake and the chemical development. The resulting photoresist profile after the development is shown in the right part of Figure 2.

The described modeling approach is used to compute standard Bossung curves. Figure 3 shows simulated Bossung data for dense and semidense lines. The dense lines have a large depth of focus (DoF). Therefore, almost no variation of the linewidth (CD) versus scanner focus position can be observed. In contrast to that the semidense lines show a pronounced variation of the CD with the defocus. The asymmetry of the Bossungs results from mask induced phase effects which result in aberration like effects. This asymmetry can already be seen in the raw AIMS™ data. A similar effect was also observed in mask topography simulations using rigorous electromagnetic field solvers and in wafer prints [17].

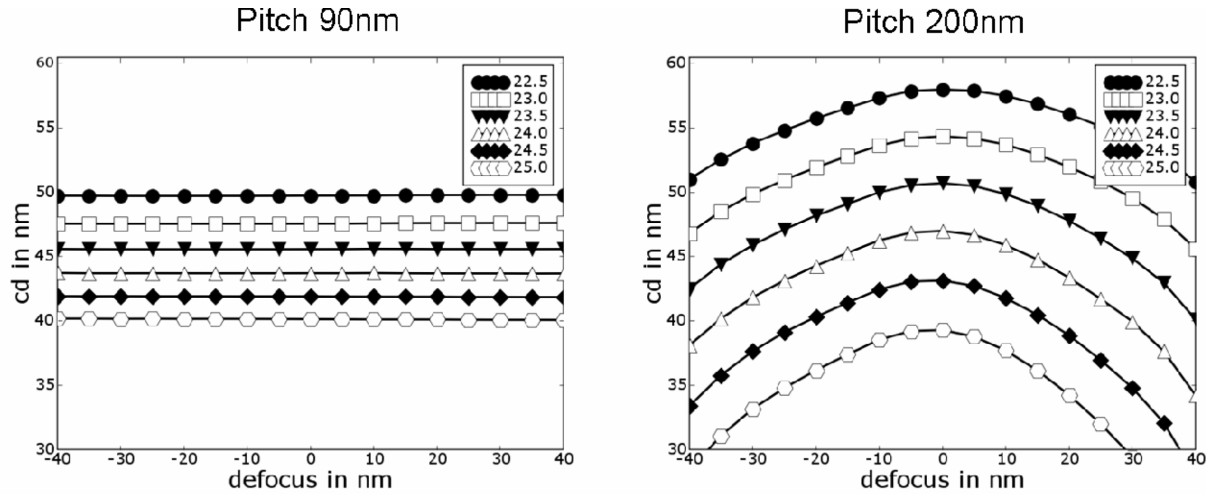

Figure 3: *Simulated Bossung curves: resist linewidth (CD) versus scanner defocus for different doses and pitches. Left: dense lines (pitch=90nm), right: semidense lines (pitch=200nm). The values in the legend boxes are the corresponding exposure doses in mJ /cm²*.

The described method to couple AIMS™ data and resist simulation neglects angular light reflections at the interfaces between the immersion liquid / photoresist and photoresist / substrate, respectively. For typical values of a photoresist refractive index of 1.7 and water immersion lithography with a numerical aperture of 1.35 the resulting error due to neglecting of the immersion liquid / resist interface will be below 2%. In lithographic applications, reflections from the photoresist / substrate interface are minimized by the application of bottom antireflective coatings.

4. RESULTS

This section compares simulation results which are obtained with the described photoresist models to actual wafer prints. To investigate the capability of the described modeling approaches to cover photoresist effects on the lithographic performance, we simulated maximum dose latitudes of line / space patterns for different pitches and compared the results to actual wafer prints. A recent publication [5] has shown that threshold model based AIMS measurements reproduce the general trend of the wafer prints very well, but show a small offset to the wafer prints.

Experimental maximum exposure latitude data were obtained from wafers printed on an ASML XT:1700i scanner (NA = 1.20 cQuad20 $\sigma_{outer}/\sigma_{inner}$ = 0.97/0.84, XY-polarized), using a binary chromium on glass (CoG) mask. We measured the maximum exposure latitude (i.e. the exposure latitude at best focus) as the relative dose latitude for which the printed wafer CD is within the nominal CD +/- 10%.

The binary CoG mask was also characterized by the AIMS™. Aerial images were measured at 11 focus steps within a focus range of 500nm in the immersion liquid. The data were passed to Dr.LiTHO and maximum dose latitudes were extracted for the specific resist models. Figure 4 shows a comparison between wafer prints, threshold model based AIMS™ measurements, and results obtained with two different typical ArF resist models.

The error bars in Figure 4 indicate the experimental error in the measurement of the wafer CD-data. The simulated CD-data were averaged over all lines within the AIMS™ field of view (see Figure 2). The resist modelling parameters of FRM1 and FRM2 were not calibrated to the specific resist which was used for the wafer prints. FRM1 has a considerably smaller diffusion length than FRM2. As can be expected, the agreement between the wafer prints and the simulation results depends strongly on the model parameters of the full resist model.

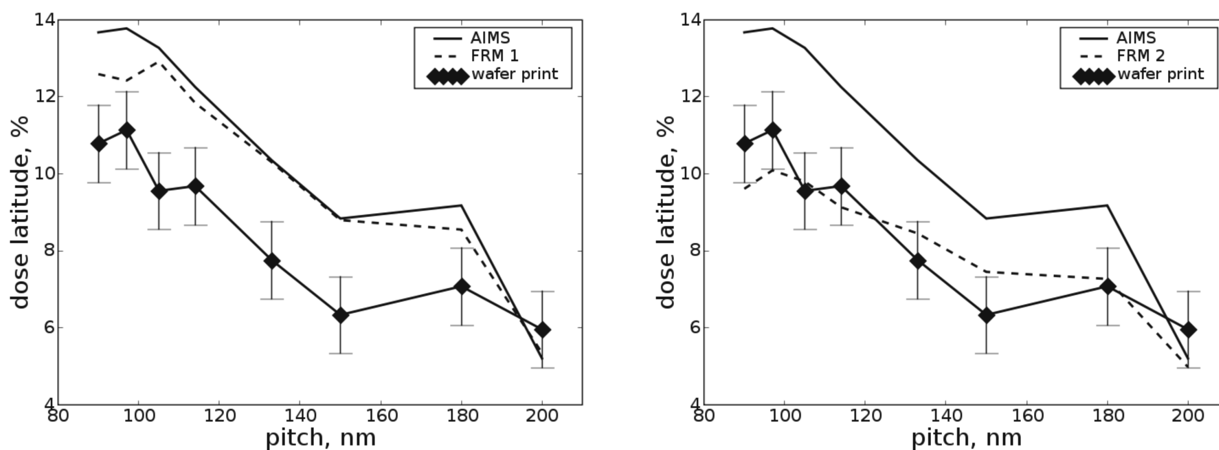

***Figure 4**: Comparison of direct AIMS™ measurements (AIMS, threshold model), wafer prints and simulation results which were obtained for typical full resist models for two 193nm-chemically amplified resists. The full resist models were not calibrated to the specific resist material and process that was used for the wafer prints. FRM1: PAR817p, FRM2: TOK TarF P6111.*

In the next step we compared the wafer print results to simulation results which were obtained with the effective acid resist model (EARM) for different modelling parameters. According to the left part of Figure 5 the diffusion length has a strong impact on the dose latitude. A diffusion length of 0nm results in almost the same dose latitude as given by the AIMS threshold model. Increasing diffusion length reduces the dose latitude and shifts the simulated data towards the error range of the wafer print data. The absolute reduction of dose latitude is more pronounced for the dense features. Therefore, the slope of the curve of dose latitude versus pitch becomes less steep with increasing diffusion lengths.

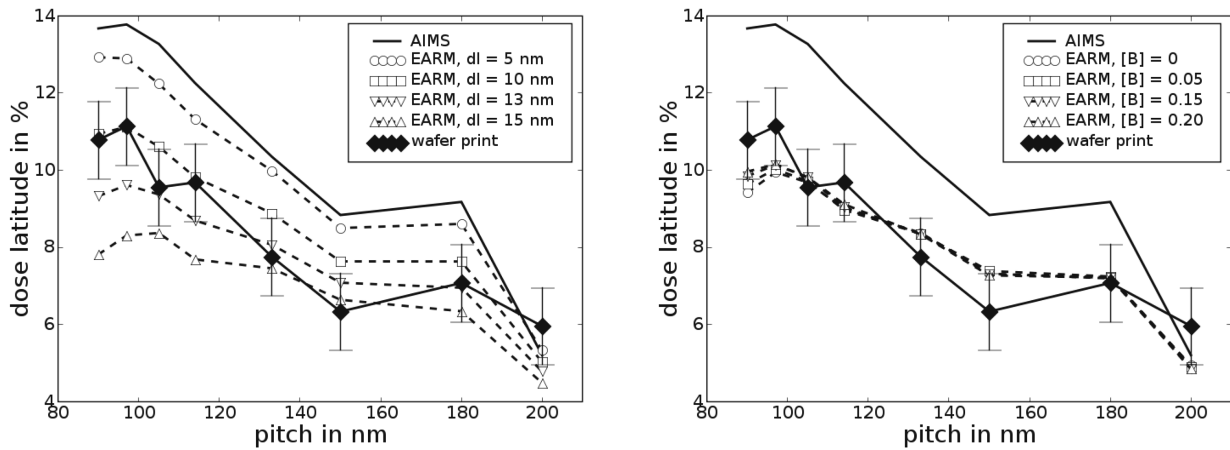

***Figure 5**: Comparison of dose latitude of direct AIMS^{TM} measurements (AIMS, threshold model), wafer prints and simulation results which were obtained with the efficient acid resist model (EARM) for different diffusion lengths dl (left) and quencher concentrations [B] (right).*

A comparison of wafer prints with EARM modelling results for different concentrations of the quencher base can be seen in the right of Figure 5. Compared to the diffusion, the quencher concentration has only a very small impact on the simulated dose latitudes. This does not imply a negligible impact of the quencher base concentration in the lithographic process. Absolute dose latitude values show a significant variation with the quencher base concentration. However, the normalization with respect to the dose to size covers these effects. Additional simulation runs demonstrated a small impact of other EARM modelling parameters such as Mack model parameters (see equation 4) on the simulated maximum exposure latitude.

Figure 6 shows a comparison between the AIMS^{TM} threshold model, wafer prints and the calibrated EARM and AIMS-CRM, respectively. A good agreement between the wafer prints and resist modelling approaches can be observed. The absolute difference between the two resist models is below 0.5%. These data clearly demonstrate the suitability of our approach to increase the predictability of AIMS^{TM} measurements.

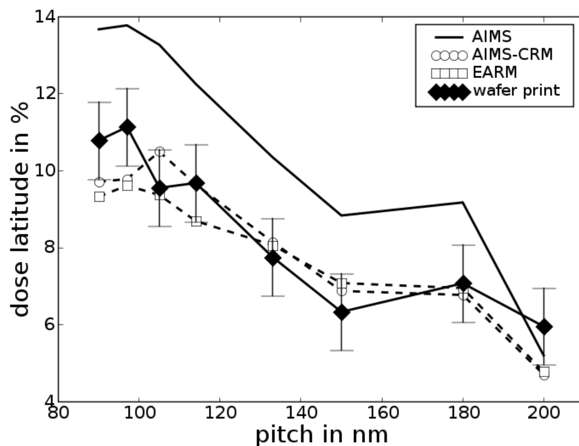

***Figure 6**: Comparison of direct AIMS^{TM} measurements (AIMS, threshold model), wafer prints and simulation results which were obtained with the calibrated efficient acid resist model (EARM) and the calibrated AIMS^{TM} compact resist model (AIMS-CRM), respectively.*

5. CONCLUSIONS AND OUTLOOK

The application of resist models to measured AIMS™ data can be used to improve the quantitative agreement between AIMS™ measurements and wafer prints. Full resist models include many parameters which are in generally not known to typical AIMS™ users and require extensive model calibration. The efficient acid resist model (EARM) and the AIMS-CRM include the essential photoresist effects like diffusion and quencher base but have considerably fewer parameters. This enables a straightforward model calibration. Also, such simplified resist models can be used in the mask house for defect analysis. Moreover, the proposed AIMS-CRM provides an excellent performance in terms of computing time.

More extensive comparisons of wafer prints and AIMS™ data based resist modeling results are required to validate the predictability of the proposed photoresist models. This has to include full Bossung curves, linearity, mask error enhancement factor (MEEF), side-lobe printing, and other lithographic process criteria.

Thus by coupling of the AIMS™ with a resist simulator we are on the way to improve the prediction and optimization of the lithographic performance of masks including defect analysis and actinic CD metrology.

REFERENCES

1. TM: Trademark of Carl Zeiss.
2. Fühner T., Schnattinger T., Ardelean G., and Erdmann A.: "Dr.LiTHO – a development and research lithography simulator", Proc. SPIE **6520** (2007) 65203F-1; www.drlitho.com.
3. See for example chapter 31 in the "Handbook of Photomask Manufacturing Technology", ed. by Syed Rizvi, Taylor & Francis, 2005.
4. Scherübl T., Dürr A.C., Böhm K., Birkner R., Richter R., and Strössner U.: "Programmed defects study on masks for 45 nm immersion lithography using the novel AIMS™45-193i", 23rd European Mask and Lithography Conference.
5. De Bisschop P., Philpsen V., Birkner R., Buttgereit U., Richter R., and Scherübl T.: "Using the AIMS 45-193i for hyper-NA imaging applications", Proc. SPIE, **6730** (2007) 67301G
6. Philipsen V., Mesuda K., De Bisschop P., Erdmann A., Citarella G., Evanschitzky P., Birkner R., Richter R., and Scheruebl T., "Impact of alternative mask stacks on imaging performance at NA 1.20 and above" Proc. SPIE, **6730**, (2007)
7. van Setten E., Grim K., Finders J., Dusa M., Birkner R., Richter R., and Scherübl T.: "Characterizing the imaging performance of Flash Memory masks using AIMS™", to be published in Proc. SPIE (2008)
8. Schnattinger T.: "Mesoscopic simulation of photoresist processing in optical lithography", PhD-Thesis, University of Erlangen-Nuremberg, 2007.
9. Erdmann A., Henke W., Robertson S., Richter E., Tollkühn B., and Hoppe W.: "Comparison of simulation approaches for chemically amplified resists", Proc. SPIE **4404** (2001) 99.
10. Robertson S., Mack C. A., and Maslow M.: "Towards a Universal Resist Dissolution Model for Lithography Simulation", Proc. SPIE **4404** (2001) 111.
11. Mack C. A.: "Development of positive photoresist", Journal of the Electrochemical Society, Solid States and Technology" **134** (1987) 148.
12. Weiss A., Binder H, and Schwalm R.: "Modeling and simulation of chemically amplified DUV resists using the effective acid concept", Microelectronic Engineering **27** (1995) 405.
13. Fuard, D., Besacier, M., and Schiavone, P.: "Validity of the diffused aerial image model: an assessment based on multiple test cases ", Proc SPIE **5040** (2003), 1536.
14. Steenwinckel D., and Van, Lammers J. H.: "Enhanced processing: sub-50nm features with 0.8 micron DOF using a binary reticle" Proc. SPIE **5039** (2003), 225.
15. Tollkühn B., Erdmann A., Lammers J., Nölscher C., and Semmler A.: "Do we need complex resist models for predictive simulation of lithographic process performance?", Proc. SPIE **5376** (2004) 983.
16. Bernard D. A.: "Simulation of Focus Effects in Photolithography", IEEE Transact. on Semicond. Manufact. **1** (1988) 85.
17. Erdmann A.: "Mask modeling in the low k_1 and ultrahigh NA regime: Phase and polarization effects", Proc. SPIE **5835** (2005) 69.